

GT2010-23114

**LP TURBINE REYNOLDS LAPSE PHENOMENA:
 TIME AVERAGED AREA TRAVERSE AND MULTISTAGE CFD**

**Matthias Kürner*, Carsten Schneider*, Martin G. Rose*, Stephan Staudacher*,
 Jochen Gier****

* Institute of Aircraft Propulsion Systems
 Stuttgart University
 Pfaffenwaldring 6
 70569 Stuttgart, Germany
 Email: matthias.kuerner@ila.uni-stuttgart.de

** MTU Aero Engines GmbH
 Dachauer Strasse 665
 80995 München, Germany

ABSTRACT

The new LP turbine test rig “ATRD” at the Institute of Aircraft Propulsion Systems (ILA) at Stuttgart University has been used to study the detailed effects of Reynolds number variation. The two-stage LP turbine has been developed in a cooperation of ILA and MTU Aero Engines GmbH. Changes in the turbine characteristics are discussed. Five hole probe area traverse data has been acquired at exit from each row of aerofoils across a broad range of Reynolds numbers, over 88,000 down to 35,000. The experimental data is supported by multi-row steady CFD predictions. The behaviour of wakes, loss cores and secondary deviations is identified across the Reynolds number range. The present study is focusing on the effects of Reynolds number variation on the vane of the second stage.

ABBREVIATIONS

ATF	Altitude Test Facility
ATRD	Advanced Turbine Research and Demonstration
ILA	Institute of Aircraft Propulsion Systems
LPT	Low Pressure Turbine
MP	Measurement Plane
MTU	MTU Aero Engines GmbH
NGV	Nozzle Guide Vanes
PS	Pressure Side
SS	Suction Side
TE	Trailing Edge

NOMENCLATURE

c	absolute velocity	[m/s]
h	specific enthalpy	[J/kg]
l/h	relative annulus height	[%]
Ma	Mach number	[-]
p	Pressure	[Pa]
R	specific gas constant	[J/(kg K)]
Re_{v1}	Reynolds number at exit of Vane 1	[-]
Re_{v2}	Reynolds number at exit of Vane 2	[-]
S	Pitch	[-]
T	Temperature	[K]
U	Circumferential Velocity	[m/s]
Y	Loss coefficient	[-]
α	circumferential flow angle	[°]
γ	isentropic exponent	[-]
δ_1	displacement thickness	[mm]
η_{is}	Isentropic Efficiency	[%]
η_{row}	Blade row efficiency	[-]

SUBSCRIPTS

1	inlet of vane 2
2	exit of vane 2
id	ideal isentropic value
is	isentropic
ref	reference value: kiel head measurement at mid span of vane 2
s	static value
t	stagnation value

1 INTRODUCTION

One major problem/challenge arises for a low-pressure turbine designer: the variation of Reynolds number over the range of applications and its resulting deteriorating impact on the turbine efficiency. As stated by Hodson and Howell [1] the Reynolds number varies in the final stage from about 50,000 at high altitude in small business jet applications to about 500,000 at sea-level takeoff. It is a well known but not entirely understood fact that losses increase by reducing the Reynolds number. The performance penalty is around 2 points for large commercial bypass engines and as much as 7 points for small, high cruise altitude, military engines as stated by Ashpis [2]. The flow field at low Reynolds numbers is dominated by laminar boundary layers, which grow faster in thickness and manifest in stronger secondary flow effects, e.g. the passage vortex or horse shoe vortices. Additionally, the boundary layer transition is postponed resulting in extended separated regions or, as the worst-case scenario, in a laminar separation without reattachment. The mentioned effects significantly increase loss and have been studied in various linear cascade tests, e.g. by Curtis et al. [3], Schulte and Hodson [4] as well as Volino [5].

A further step towards simulating realistic flow conditions in engines is to run the entire LP turbine under high altitude flight conditions – the so called “turbine rig”. Keeping the Mach number and the Reynolds number analogy by embedding the turbine rig in an altitude test facility leads to a high grade of realism in the turbomachinery flow. This includes mass flow redistribution due to streamline curvature, leakage flow and secondary flow effects. In the past only few results of turbine rigs, which achieve the mentioned aspects, have been published. Some of them are: Gier and Ardey [6], Haselbach et al. [7], Howell et al. [8] and Gier et al. [9]. The authors address LP turbine flow phenomena in the Reynolds number range of approximately 90,000 to 550,000.

This paper presents the effects of low Reynolds number on the flow field of NGV2 of a two-stage LP turbine by showing results of aerofoil statics located on three streamlines (hub, mid and tip) and 30x30 points five hole probe area measurement data of the exit flow field covering 1.1 pitches. Three operating points are investigated covering a Reynolds number range from 35,000 to 88,000. The Reynolds number is based on the exit velocity and the true chord length of NGV2. The experimental results are supported by multi-stage steady CFD calculations.

2 DESCRIPTION OF THE TURBINE TEST RIG

The ATRD-Rig is a two-stage low pressure axial turbine developed to fundamentally improve the understanding of the flow behavior at low Reynolds numbers in turbomachinery. By using the Altitude Test Facility (ATF) at the Institute of Aircraft Propulsion Systems (ILA) at Stuttgart University, the turbine demonstrator can be operated in the Reynolds number regime down to approximately $Re_{V2}=35,000$. The possibility of adjusting the Reynolds number allows preserving Mach and Reynolds analogy in the turbine flow and consequently leads to

almost realistic flow features compared to a LP turbine driven in an engine at high altitude. The rig embedded in the ATF is shown in Fig. 1. A more detailed description of the ATRD-Rig can be found in Schinko et al. [10].

The actual setup of the ATRD-Rig is one build of a long term measurement campaign. A general arrangement of the turbine including the analysis relevant measurement planes (MP: 4, 9 and 13) and leakage paths are given in Fig. 2. Leakage flow paths are indicated by arrows. The turbine blades are designed with conventional blade loading and aspect ratio (e.g. NGV2: 2.57) to give the opportunity to compare with state-of-the-art aft-loaded turbine blade designs. On average, the absolute Mach number at exit of each blade row is about 0.45 and stage loading $\Delta h_r/U^2$ is slightly above two. The radius ratio from exit NGV1 to exit NGV2 is 1.18 and leads to an average flare angle of approximately 17° . To create the required swirl in the inlet plane (MP4) an adjustable IGV with 120 vanes is installed upstream.

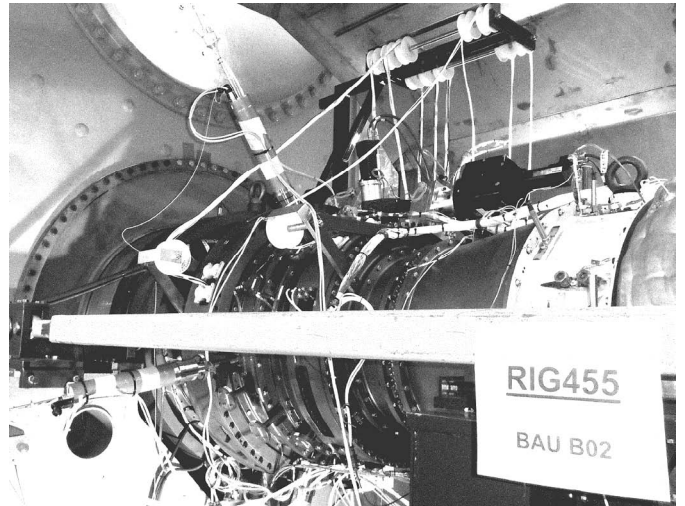


Fig. 1 ATRD-Rig mounted on the ATF of Stuttgart University

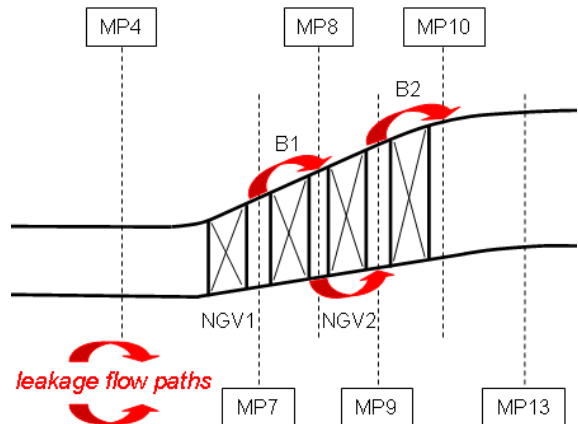


Fig. 2 Schematic sketch of the two-stage turbine including measurement planes

3 EXPERIMENTAL METHODS

As an indication for the overall reduction of the turbine efficiency due to low Reynolds Number effects, the isentropic efficiency η_{is} based on the stagnation flow values of the inlet (MP4) and the exit (MP13) of the turbine is used. It is defined as

$$\eta_{is} = \frac{h_{t,4} - h_{t,13}}{h_{t,4} - h_{t,13,is}} \quad (1)$$

with the variable h_t ($h_{t,is}$) representing the specific stagnation (isentropic) enthalpy in the relevant planes. The gas properties are generally humidity corrected. As inlet area traversing in MP4 was not performed at all operating conditions, an interpolation procedure using a loss coefficient is used to provide the missing data for the stagnation pressure p_t and stagnation temperature T_t in MP4. The result of the interpolation procedure is in agreement with the five hole probe measurement.

In MP13, p_t and T_t are measured with three rakes each. In both cases the rakes have ten kiel heads radially distributed with higher resolution in the secondary flow area at hub and tip. The circumferential distribution of the rakes is not equidistant to resolve the circumferential flow distortion. Detailed information about rake measurement in turbomachinery can be found in Saravanamuttoo [11].

In MP 7 to MP 10 five hole probe measurements and two component hot film probe area measurements have been carried out. This paper is focusing on the steady data analysis of the NGV2 exit (MP9). Accordingly, the five hole probe area measurement method is briefly presented. The measurement grid resolution is 30x30 points covering 1.1 pitches over a relative annulus height of 0.43% to 94.6%. In circumferential direction, the grid points are spaced equidistant in angle whereas in radial direction, the resolution within the secondary flow areas has been improved by reducing the number of grid points in the 2D flow dominated region at mid height of the annulus. The measurement grid is shown in the contour plots, e.g. see Fig. 10. The flow variables measured with the five hole probe are mass-averaged except for static pressure, which is area-averaged, according to Cumpsty and Horlock [12].

4 COMPUTATIONAL METHOD

CFD-calculations have been carried out using the commercial flow solver Ansys CFX 12 using SST turbulence model and Langtry-Menter transition model. A hybrid mesh was created using Centaur with structured hex-elements for boundary layer resolution and tetrahedral elements for the rest of the domain. Local mesh refinements have been performed to resolve local flow structures. The mesh contains about 8 million nodes. Leakage paths are not included in the CFD-calculations. Boundary conditions for the inlet are taken from five hole probe area measurements in MP4 in combination with the

interpolation procedure. For the exit boundary condition five hole probe measurements in MP13 are used.

5 EXPERIMENTAL AND NUMERICAL RESULTS

5.1 TURBINE CHARACTERISTICS

In Fig. 3 the turbine characteristic of isentropic efficiency over Reynolds number is shown. The characteristic exhibits a considerable trend towards lower efficiency, indicating increasing losses with lower Reynolds number. Over the Reynolds number range the isentropic turbine efficiency is found to drop by 2.4%. CFD is in reasonably close agreement with a deterioration of 2.8%. The absolute level of the losses predicted by CFD is less accurate ($\Delta\eta \approx +2\%$). Neglecting leakage flow in the CFD-prediction is one reason for the difference in efficiency.

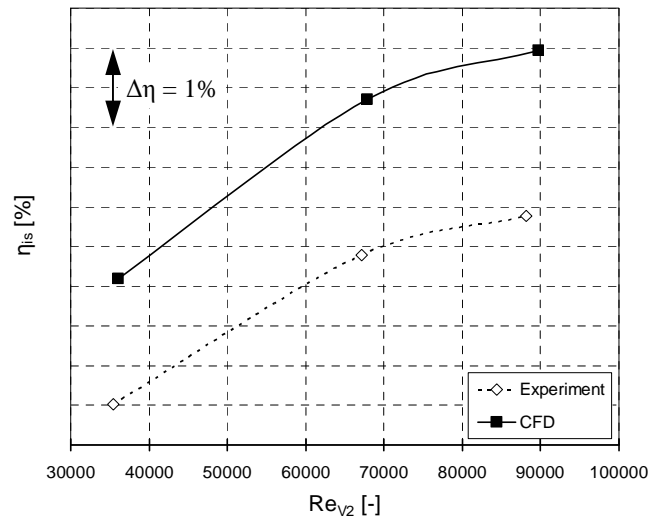


Fig. 3 Turbine characteristic: η_{is} over Re_{v2}

5.2 IDENTIFICATION OF LOSSES

Laminar boundary layer separation is a well known source of loss in low pressure turbines, especially at low Reynolds number conditions. In Fig. 4 to Fig. 6 the aerofoil pressure distribution of experimental and CFD-predicted data is shown for the three Reynolds numbers. The reference pressure $p_{t,ref}$ is measured by a kiel head on the leading edge at mid span of vane 2. The experimental results of the three operating conditions are summarized in Fig. 7. Both experimental and numerical results are in good agreement and show an increasing separation bubble on the suction side with lower Reynolds number. This behaviour is in agreement with various LPT aerofoil cascade tests as reported by Schulte and Hodson [4] or Volino [5].

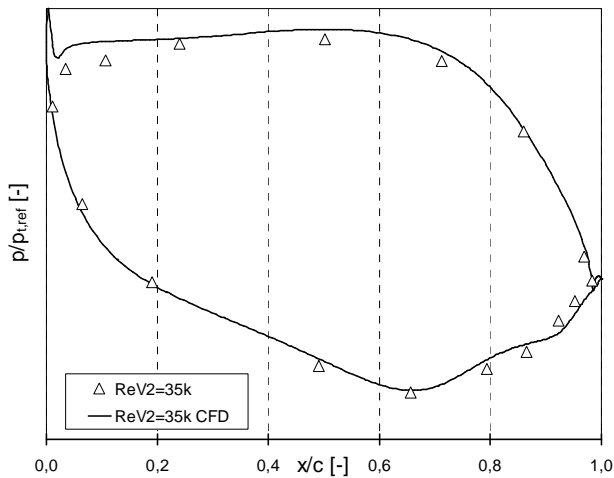


Fig. 4 Aerofoil pressure distribution on vane 2 at midspan, $Re_{V2}=35,000$

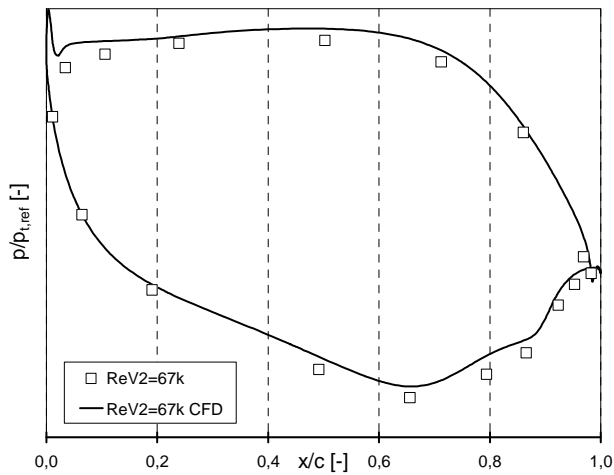


Fig. 5 Aerofoil pressure distribution on vane 2 at midspan, $Re_{V2}=67,000$

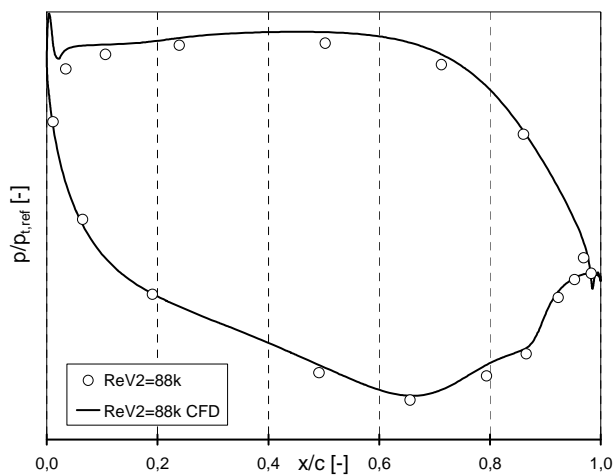


Fig. 6 Aerofoil pressure distribution on vane 2 at midspan, $Re_{V2}=88,000$

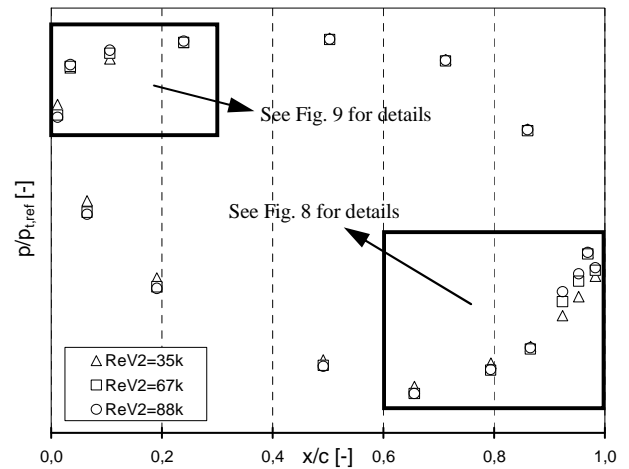


Fig. 7 Measured aerofoil pressure distribution on vane 2 at midspan

A magnified view for the pressure distribution on the rear part of the suction side is presented in Fig. 8, where the different bubble sizes and reattachment points due to Reynolds number variation can be identified. For all operating points, transition very likely occurs in the separation zone and the turbulent boundary layer reattaches before reaching the trailing edge.

A second separation zone can be identified on the pressure side directly behind the leading edge. A detailed view of the leading edge pressure side region is given in Fig. 9. The size of the leading edge separation is as well increasing with lower Reynolds number, following the observed trend on the suction side separation zone. In the steady CFD-prediction, this effect is more pronounced than in the experimental data. It is supposed, that unsteady flow effects like varying incidence and hysteresis (e.g. observed in unsteady helicopter aerodynamics) influence the leading edge flow field and reduce the separation in a time-averaged point of view. It is unlikely to be unsteady transition, as the distance from the stagnation point to the separation point is too short to allow for transition. More information about transition mechanisms in turbomachinery can be found in Mayle [13].

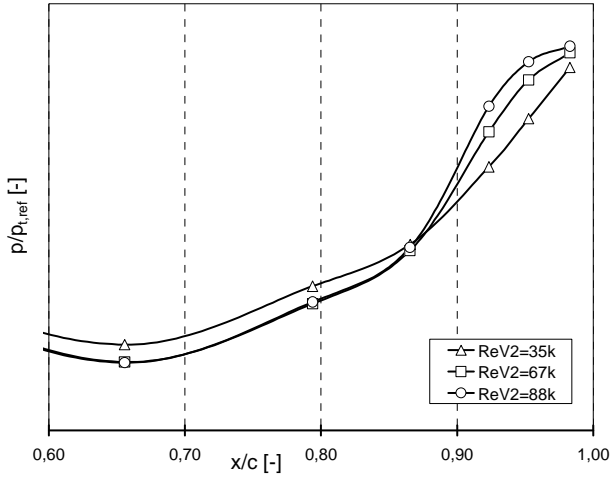


Fig. 8 Measured aerofoil pressure distribution on vane 2 at midspan to show laminar separation bubble with turbulent reattachment on the suction side

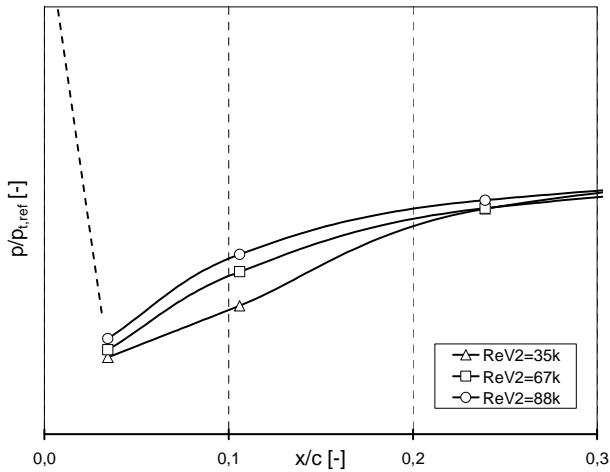


Fig. 9 Measured aerofoil pressure distribution on vane 2 at midspan to show leading edge pressure side separation

Besides changes in separation regions, secondary flow and wake thickness is expected to increase with lower Reynolds number. In Fig. 10 to Fig. 12 the blade row efficiency η_{row} based on five hole probe measurements at exit of vane 2 (MP9) is shown on the left hand side of the figures. CFD-predicted data is presented on the right hand side. The blade row efficiency is defined as

$$\eta_{row} = \left(\frac{c_2}{c_{2,id}} \right)^2 \quad (2)$$

$$c_{2,id} = \sqrt{Ma_{id}^2 \cdot \gamma \cdot R \cdot T_{t,ref} \left(\frac{1}{1 + \frac{\gamma-1}{2} \cdot Ma_{id}^2} \right)} \quad (3)$$

$$Ma_{id}^2 = \frac{2}{\gamma-1} \left[\left(\frac{p_{t,ref}}{p_2} \right)^{\frac{\gamma-1}{\gamma}} - 1 \right] \quad (4)$$

with $c_{2,id}$ being the ideal isentropic exit velocity. $T_{t,ref}$ and $p_{t,ref}$ are obtained using kiel heads on the leading edge of vane 2 at midspan ($l/h \approx 50\%$). The blade row efficiency is used to identify loss cores and wakes. In this paper blade row efficiency is favoured over loss coefficient (such as given by Denton [14])

$$Y = \frac{p_{t1} - p_{t2}}{p_{t2} - p_2} \quad (5)$$

Loss coefficient Y is a function of total pressure difference at inlet and exit of the blade row over exit dynamic head. The advantage of using blade row efficiency is that it takes pressure and temperature changes into account when evaluating loss.

The contour plots, both experimental and CFD-prediction, show the expected trend of Reynolds number influence: loss cores and wakes grow in size with lower Reynolds number. The radial positions of the loss cores are nearly insensitive to Reynolds number. At $Re_{v2}=35,000$, an additional loss region can be observed in the wake at a relative annulus height l/h of about 14 to 21%. The additional loss core will be subject of future analysis. Furthermore, there is evidence for stronger radial inward migration in the wake region at $l/h \approx 80\%$ compared to the other cases. Both features are not clearly visible in the CFD-prediction. For $Re_{v2}=67,000$ and $Re_{v2}=88,000$ a local decrease of η_{row} is visible at about 57% relative annulus height in the experimental data, indicating a flow structure of vane 1. This structure might be the passage vortex of vane 1 or the rolled up wake of it. The effect is more pronounced the higher the Reynolds number is. This is due to stronger mixing at lower Reynolds numbers, allowing the flow structure to mix out more completely. This effect is not visible in the CFD-prediction due to the mixing-plane approach used for the steady multi-row calculations.

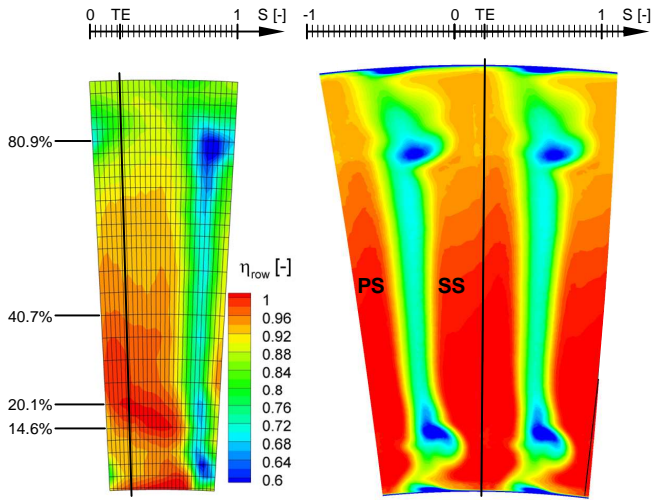


Fig. 10 Contour plot of η_{row} at exit of vane 2; $Re_{v_2}=35,000$; left: experimental data; right: CFD

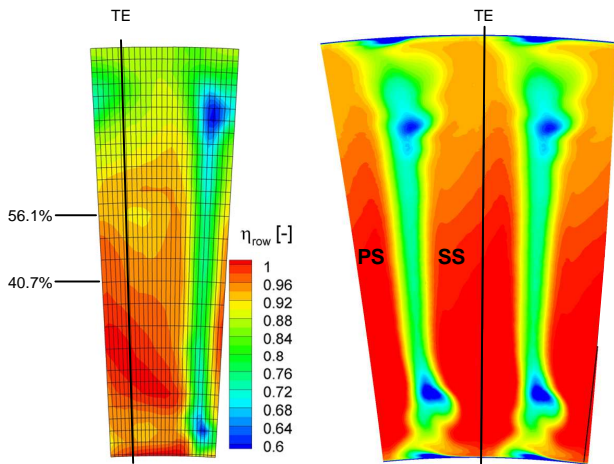


Fig. 11 Contour plot of η_{row} at exit of vane 2, $Re_{v_2}=67,000$; left: experimental data; right: CFD

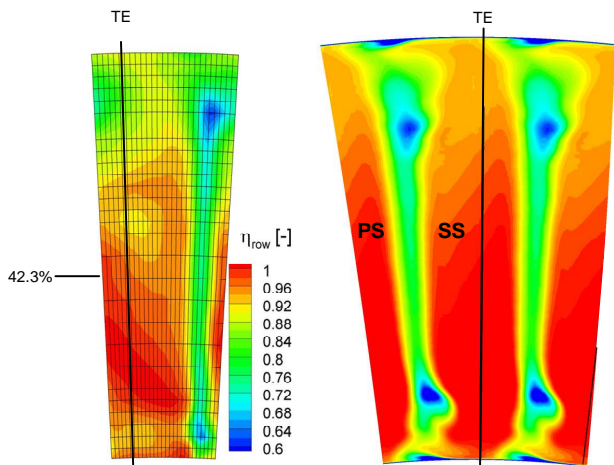


Fig. 12 Contour plot of η_{row} at exit of vane 2, $Re_{v_2}=88,000$; left: experimental data; right: CFD

As a consequence to the growing separations presented earlier, the wake thickness increases significantly in the 2D-flow dominated area around midspan. In Fig. 13, the circumferential distributions of blade row efficiency at about 41% relative annulus height are shown for the three operating conditions. This annulus height is chosen because the previously mentioned flow structure at $l/h \approx 57\%$ leads to a distortion of the quasi 2D-flow at midspan. The velocity defect due to the wake is clearly visible. Aperiodicity is visible in the circumferential distribution of η_{row} which can be explained by the different blade numbers for stator 1 and stator 2 (ratio=1.034) and measurement uncertainties. Remarkably, the degree of aperiodicity is increasing with decreasing Reynolds numbers. At $Re_{v_2}=88,000$, the flow is almost periodic whereas at $Re_{v_2}=35,000$, the difference of η_{row} between $S=0$ and $S=1$ is about 3.5%. As the same probe and tubing was used for the measurement, this phenomenon is supposed to be real flow behaviour and not a problem with the instrumentation. The kink at $Re_{v_2}=35k$ and $S \approx 0.45$ is expected to be a measurement error. The results of the numerical simulation are shown in Fig. 14. On account of clarity, in the CFD result plots every tenth data point is marked by a symbol. Blade row efficiency numbers larger than unity are due to the following simplifications: a) the neglected radial gradient of total pressure and total temperature at inlet of vane 2, b) the selected reference values for $T_{t,ref}$ and $p_{t,ref}$ at the leading edge of vane 2 at a single height $l/h \approx 50\%$ and c) ignoring radial migration. In the free stream region, blade row efficiency is overestimated by CFD. In contrast to the experiment, only a slight variation of the blade row efficiency level is shown in this region for the three operating points. The wake region is predicted at a slightly lower pitch value. However, the trend in reducing wake thickness and amplitude with increasing Reynolds number can be clearly seen in the CFD results.

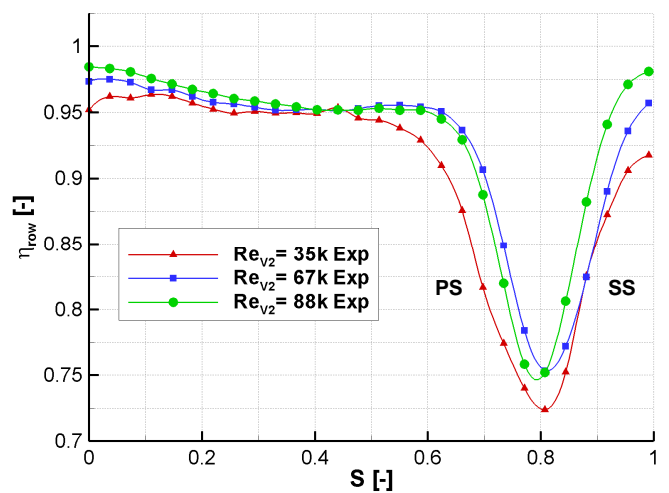


Fig. 13 Circumferential variation of η_{row} at vane 2 exit, midspan region: $l/h=40,7\%$ ($Re_{v_2}=35k$, $Re_{v_2}=67k$), $l/h=42,3\%$ ($Re_{v_2}=88k$); experimental data

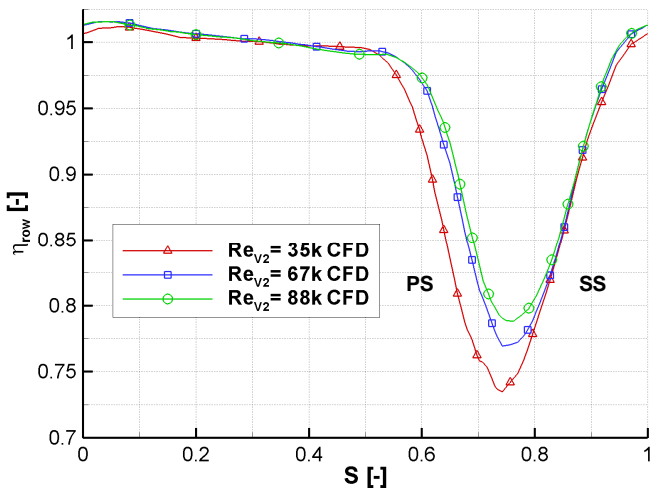


Fig. 14 Circumferential variation of η_{row} at vane 2 exit, mid span region: $l/h=40,7\%$ ($Re_{v2}=35k$, $Re_{v2}=67k$), $l/h=42,3\%$ ($Re_{v2}=88k$); CFD data; every tenth data point marked

To quantify the increased wake thickness and amplitude, the displacement thickness δ_1

$$\delta_1 = \int_0^S \left(1 - \frac{c}{c_{id}} \right) ds \quad (6)$$

is calculated by using one pitch as integration length at exit of vane 2. Here, the displacement thickness is used because it is an integral parameter and therefore more reliable than a single value. As the true free stream velocity is difficult to identify, the ideal isentropic velocity (see equation (3)) is chosen as free stream velocity. The results of the integration are given as relative numbers $\delta_1/\delta_{1,Re=88k}$ in Fig. 15 with $\delta_{1,Re=88k}$ as the displacement thickness at $Re_{v2} = 88,000$ for measured data and CFD-data, respectively. For the high Reynolds number case no measurement at relative annulus height 40.7% is available. Therefore, the adjacent radius with $l/h=42.3\%$ is chosen. The difference due to that radius change is expected to be minor, since these radial positions are in the 2D-flow region of the vane.

In the midspan region, where the flow is behaving in a quasi-2D manner, a clear trend is visible for increasing δ_1 with lower Reynolds number. The displacement thickness in the experiment is increased by 8.0% for $Re_{v2}=67,000$ and by 37.6% for $Re_{v2}=35,000$. The CFD-results for the distribution of the relative displacement thickness do show the same trend as in the experiment. The relative results are in good agreement with the experimental data, though the increase of $\delta_1/\delta_{1,Re=88k}$ for the lowest Reynolds number is overestimated by 2.4%. However, the absolute numbers show a large error (cf. Fig. 13 and Fig. 14).

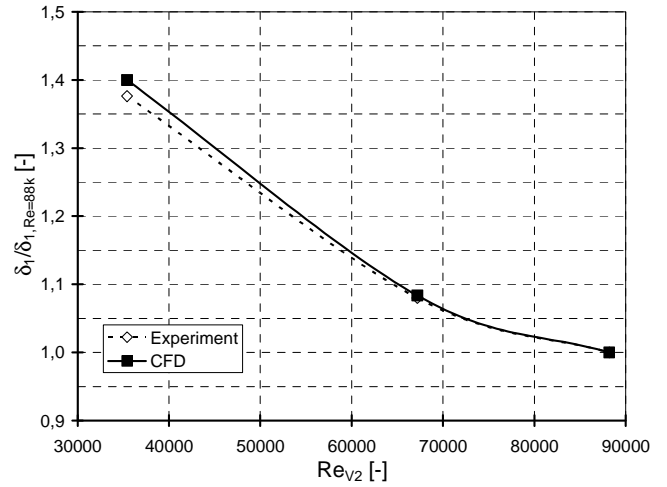


Fig. 15 Relative displacement thickness of wake and loss cores at different Reynolds numbers at about 41% relative annulus height

In Fig. 16 the circumferential distribution of the total pressure ratio is given. Higher blade row efficiency and higher total pressure towards the suction side at the exit of the vane 2 are evidence of the unsteady work processes as the wake of rotor 1 interacts with vane 2, as described by Hodson and Dawes [15].

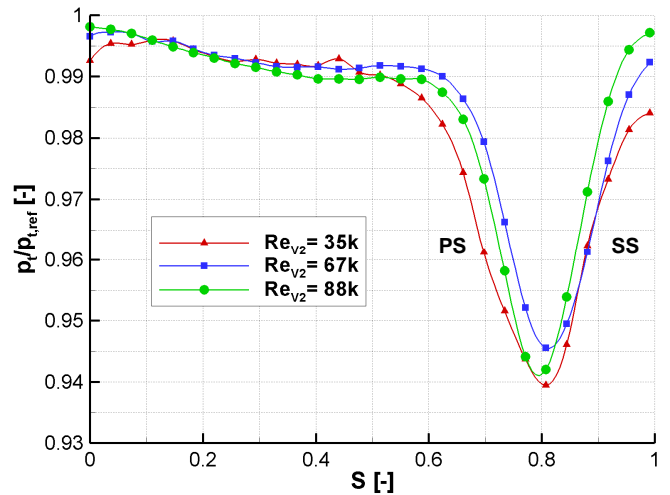


Fig. 16 Circumferential variation of $p_t/p_{t,ref}$ at vane 2 exit, mid span region: 41% relative annulus height (for comparison with Hodson and Dawes [15])

In Fig. 17 the experimentally derived radial distribution using five hole probe data of blade row efficiency η_{row} at exit from vane 2 is shown. The data is mass-averaged. In the region from 15% to 55% of the relative annulus height, the loss is dominated by 2D-aerofoil loss. The gradient of the blade row

efficiency in this region is due to the selection of the reference pressure $p_{t,ref}$ and reference temperature $T_{t,ref}$ in the definition of η_{row} in equation (2) to (4): these reference values are derived from a single kiel head at midspan of the leading edge of vane 2. Therefore, the radial variation of total pressure and total temperature at inlet of vane 2 is not taken into account. This results in pseudo-losses leading to a gradient in the radial distribution. The blade row efficiency is continuously decreasing with lower Reynolds number due to the previously described increased separation regions. At mid span, η_{row} diminishes by 0.6% for $Re_{v_2}=67,000$ and 2.6% for $Re_{v_2}=35,000$ relative to the high Reynolds number case. The differences of η_{row} for the three operating points throughout 15% to 55% relative annulus height are nearly constant. The CFD-prediction, as presented in Fig. 18, overestimates η_{row} by about 3%. At mid span, the CFD-predicted η_{row} diminishes by 0.5% for $Re_{v_2}=67,000$ and 1.9% for $Re_{v_2}=35,000$ relative to the high Reynolds number case. The local decrease of η_{row} in the experimental data at about 57% relative annulus height indicates a flow structure of vane 1 as previously identified in Fig. 11 and Fig. 12. The quantitative variation of this effect due to Reynolds number change can be clearly seen in the radial distribution of η_{row} . It almost disappears for the lowest Reynolds number case. In the endwall region, the flow field is strongly influenced by secondary flow features (passage vortex vane 2, horseshoe vortex vane 2, trailing shed vortex vane 2) leading to lower efficiency numbers. CFD predicts strong variation of the loss of the casing vortex system for the different Reynolds numbers whereas the experiment shows little variation. For the experimental data it is suspected that higher turbulence in the endwall region leads to more stable flow structures being less sensitive to Reynolds number variation. Similar loss behaviour is observed in the hub region but the flow field at the hub is additionally influenced by leakage. As leakage is not included in the CFD calculations, additional information can not be derived. These effects will be the subject of further research. To quantify the region influenced by leakage, the circumferential flow angle distribution at MP9 is given in Fig. 19. Up to approximately 9% relative annulus height a significant underturned flow region can be observed, indicating the region of leakage influence. The influence of leakage is insensitive to Reynolds number changes across the observed range. Leakage is known to have lower circumferential velocity than the NGV exit flow and leakage is likely to be the reason for the rising blade row efficiency numbers towards the hub (relative annulus height < 7%) in the experimental data.

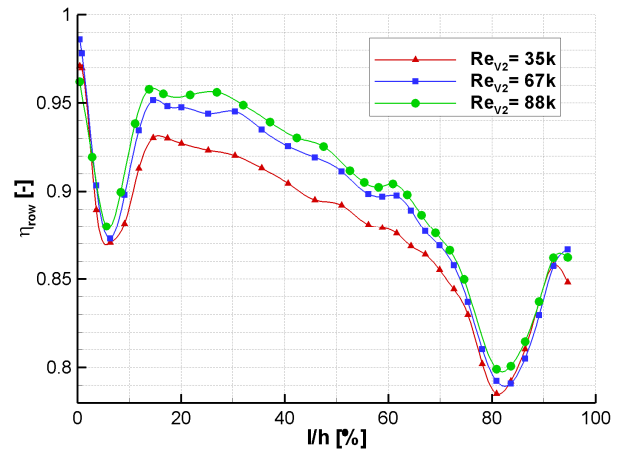


Fig. 17 Radial distribution of η_{row} at exit of vane 2: Experimental data

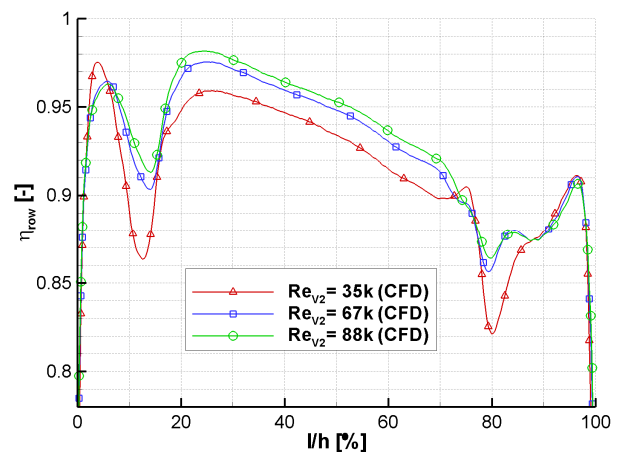


Fig. 18 Radial distribution of η_{row} at exit of vane 2: CFD-prediction; every tenth data point marked

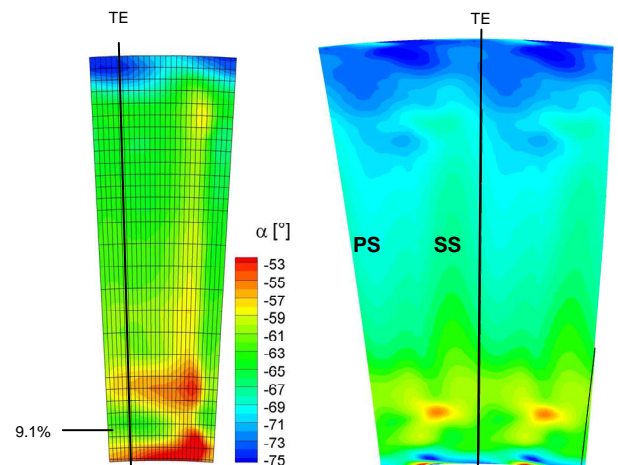


Fig. 19 Contour plot of yaw angle α at exit of vane 2, $Re_{v_2}=35,000$; left: experimental data; right: CFD

6 CONCLUSIONS

The ILA–MTU ‘ATRD’ turbine rig, a two-stage model of a typical aero-engine LP turbine, has been tested over a broad range of Reynolds number (35,000 to 88,000). This paper reports on detailed area traverse data, aerofoil statics and CFD simulation of the NGV of the second stage.

Over the Reynolds number range the isentropic turbine efficiency is found to drop by 2.4%. CFD is in reasonably close agreement with a deterioration of 2.8%. The absolute level of the losses predicted by CFD is less accurate ($\Delta\eta \approx +2\%$), principally because flow leakage has been neglected in these calculations.

NGV2 features local flow separations on both early pressure side and late suction side. The surface static pressure measurements reveal changes due to the Reynolds number reduction. There is evidence of both earlier separation and later transition. The area traverse data clearly shows significant changes as Reynolds number is reduced; wakes get wider, loss cores get larger and a new loss core appears at the lowest Reynolds number (35,000). The increase in the wake is reflected in an increase of wake displacement thickness of 38% from maximum to minimum Reynolds numbers. At vane 2 exit the free stream fluid at midspan has higher total pressure towards the suction side of the vane. This is evidence of the unsteady work processes as the wake of rotor 1 interacts with vane 2.

Some time average flow distortions in the vane 2 exit traverse data are found. These have their origins in vane 1: the strength of these distortions diminishes with reducing Reynolds number. It is thought likely that the reason for this is the increased mixing due to reduced Reynolds number.

Much more experimental data is available from the ATRD rig, with area traverses at exit from all rows with 5-hole and twin film probes and spanning the range of the characteristic. Subsequent publications will offer interpretation of this large data set.

ACKNOWLEDGMENTS

The presented paper was developed in terms of the Advanced Turbine Research and Demonstration Project. This cooperation project between MTU and ILA was launched as a result of the Turbine Competence Centrum founded in 2006 between MTU and Stuttgart University.

The authors would like to express their gratitude to the whole MTU Company for their support and the possibility to publish the gained know-how resulting from the cooperation project.

REFERENCES

- [1] Hodson, H.P.; Howell, R.J.: “Bladerow Interactions, Transition, and High-Lift Aerofoils in Low-Pressure Turbines”, *Annu. Rev. Fluid Mech.*, 2005, Vol. 37
- [2] Ashpis, D.E.: “The NASA Low-Pressure Turbine Flow Physics Program: A Review”, *Minnowbrook III: 2000 Workshop on Boundary Layer Transition and Unsteady Aspects of Turbomachinery Flows*, 2002
- [3] Curtis, E.M.; Hodson, H.P.; Banieghbal, M.R.; Denton, J.D.; Howell, R.J.; Harwey, N.W.: “Development of Blade Profiles for Low-Pressure Turbine Applications”, *Journal of Turbomachinery*, 1997, Vol. 119
- [4] Schulte V.; Hodson, H.P.: “Unsteady Wake-Induced Boundary Layer Transition in High Lift LP Turbines”, *Transactions of the ASME*, 1998, Vol. 120
- [5] Volino, R.J.: “Separated Flow Measurements on a Highly Loaded Low-Pressure Turbine Airfoil”, *Journal of Turbomachinery*, 2010, Vol. 132
- [6] Gier, J.; Ardey, S.: “On the Impact of Blade Count Reduction on Aerodynamic Performance and Loss Generation in a Three-Stage LP Turbine”, *Proceedings of ASME*, 2001-GT-0197
- [7] Haselbach, F.; Schiffer, H.-P.; Horsman, M.; Dressen, S.; Harwey, N.W.; Read, S.: “The Application of Ultra High Lift Blading in the BR715 LP Turbine”, *Journal of Turbomachinery*, 2002, Vol. 124
- [8] Howell, R. J.; Hodson, H.P.; Schulte, V.; Stieger, R.D.; Schiffer, H.-P.; Haselbach, F.; Harvey, N.W.: “Boundary Layer Development in the BR710 and BR715 LP Turbines – The Implementation of High-Lift and Ultra-High-Lift Concepts”, *Journal of Turbomachinery*, 2002, Vol. 124
- [9] Gier, J.; Franke, M.; Hübner, N.; Schröder, T.: “Designing LP Turbines for Optimized Aitfoil Lift”, *Proceedings of ASME*, GT2008-51101
- [10] Schinko, N.; Kürner, M.; Staudacher, S.; Rose, M.G.; Gier, J.; Raab, I.; Lippl, F.: “Das ATRD-Projekt - Ein Beispiel für die Zusammenarbeit von Industrie und Universität zur Förderung der Grundlagenforschung“, *DGLR Congress, DLRK2009 121156*, Aachen 2009
- [11] Saravanamuttoo, H.I.H.: “Recommended Practices for Measurement of Gas Path Pressures and Temperatures for Performance Assessment of Aircraft Turbine Engines and Components”, *AGARD Advisory Report No. 245*, 1990
- [12] Cumpsty, N.A.; Horlock, J.H.: “Averaging Nonuniform Flow for a Purpose”, *Transactions of the ASME*, 2006, Vol. 128
- [13] Mayle, R.E.: “The Role of Laminar-Turbulent Transition in Gas Turbine Engines”, *Journal of Turbomachinery*, 1991, Vol. 113
- [14] Denton, J.D.: “Loss Mechanisms in Turbomachines”, *Journal of Turbomachinery*, 1993, Vol. 115
- [15] Hodson, H.P.; Dawes, W.N.: “On the interpretation of measured profile losses in unsteady wake-turbine blade interaction studies”, *Journal of Turbomachinery*, 1998, Vol. 120